Asian Journal of Chemistry; Vol. 38, No. 3 (2026), 665-673
ASIAN JOURNAL OF CHEMISTRY
https://doi.org/10.14233/ajchem.2026.35248

Development of Coconut Shell Derived Nanobiochar as High-Efficient Adsorbent for Removal of Congo Red and Malachite Green from Wastewater

VASAMSETTI SAI SRUTHI[1], J. ARAVIND KUMAR[2,*] and VEERAMALLI NAVEEN SAHITH[1]

[1]Department of Biotechnology, Saveetha School of Engineering, Saveetha Institute of Medical and Technical Science, SIMATS, Chennai-602105, India
[2]Department of Energy and Environmental Engineering, Saveetha School of Engineering, Saveetha Institute of Medical and Technical Science, SIMATS, Chennai-602105, India

*Corresponding author: E-mail: aravindkumarj.sse@saveetha.com

Received: 13 November 2025 *Accepted*: 13 January 2026 *Published online*: 6 March 2026 AJC-22286

This study presents an innovative approach for the efficient removal of Congo red (CR) and malachite green (MG) dyes from wastewater using coconut shell-derived nanobiochar (NBC). The NBC was synthesised *via* a two-step process involving controlled pyrolysis, KOH activation and ball milling to achieve nanoscale dimensions, thereby enhancing its adsorption performance. The resulting NBC demonstrated exceptional dye removal capabilities, with maximum adsorption capacities of 220 mg g^{-1} for MG and 140 mg g^{-1} for CR under optimal conditions. Comprehensive characterisation using X-ray diffraction (XRD), Fourier-transform infrared spectroscopy (FTIR) and dynamic light scattering (DLS) confirmed the high surface area (400 m^2 g^{-1}), negative zeta potential (-30.8 mV) and superior dispersion stability of NBC material, which are essential for efficient dye adsorption. The adsorption kinetics were well-described by the pseudo-second-order model suggesting that chemisorption is the predominant adsorption mechanism. Thermodynamic analysis indicated that the adsorption process is both spontaneous and endothermic. These findings highlight the potential of NBC as a cost-effective, scalable and sustainable adsorbent for dye-laden wastewater treatment. The study also demonstrates the feasibility of utilizing coconut shell waste as a renewable biomass resource, contributing to environmental remediation while promoting circular economy practices.

Keywords: Nanobiochar, Coconut shell, Dye adsorption, Malachite green, Congo red, Wastewater treatment.

INTRODUCTION

Water pollution has become one of the most critical global challenges of the 21st century, with industrial wastewater being a primary contributor to environmental degradation. Among the numerous pollutants, synthetic dyes are particularly concerning due to their widespread use, toxicity and persistence in aquatic ecosystems [1]. Synthetic dyes constitute a significant category of environmental pollutants, with global production exceeding 700,000 metric tons annually and more than 10,000 distinct commercial varieties in widespread use [2]. Dyes such as Congo red and malachite green, which are commonly employed in the textile, paper and leather industries, are particularly problematic due to their intense colour and chemical stability. These dyes, prized for their vibrant colours and durability, persist in the environment for extended periods, making their removal from wastewater a crucial environmental challenge [3]. When these dyes are released into the environment, they pose severe threats to water quality, aquatic organisms and human health [4]. The primary concern is their resistance to natural degradation processes, which results in their accumulation in water bodies, leading to oxygen depletion, disruption of photosynthetic activities and severe toxicity to aquatic life. Moreover, these dyes have been linked to mutagenic, carcinogenic and neurotoxic effects on both aquatic organisms and humans, making their removal from wastewater an urgent and critical issue [5]. Conventional wastewater treatment methods, such as coagulation, flocculation and biological processes, have long been used to address this problem. However, these techniques often face challenges in efficiently removing synthetic dyes, particularly those with complex chemical structures and high concentrations [6]. They also typically involve high operational costs, large quantities of chemicals and the generation of secondary waste, which

makes them less sustainable and effective in the long run. As a result, there has been growing interest in developing more efficient, cost-effective and eco-friendly approaches to treat dye-laden wastewater [7].

Among the emerging alternatives, adsorption has gained significant attention as a promising technique for the removal of dyes from wastewater due to its simplicity, efficiency and cost-effectiveness. The process involves the attachment of dye molecules onto the surface of adsorbent materials and it offers several advantages, including high removal efficiency, minimal energy consumption and the potential for regenerability [8]. Conventional adsorbents, such as activated carbon, clay and zeolites, have been extensively studied for dye removal. While activated carbon, for instance, is highly effective due to its large surface area and microporous structure, its high production cost and limited reusability have hindered its widespread use in large-scale applications [9]. This has led to the exploration of more sustainable and cost-effective adsorbents derived from renewable resources.

In recent years, biochar, a carbon-rich material produced from the pyrolysis of organic waste, has emerged as a promising alternative. Biochar is not only abundant and low-cost, but it also has a high surface area, making it suitable for adsorption applications [10,11]. Although biochar has demonstrated good dye adsorption capabilities, however, its performance is often limited by its relatively low surface area and slow adsorption kinetics [12]. To overcome these limitations, the field of nanotechnology has introduced exciting possibilities by engineering biochar at the nanoscale. Nanobiochar, a modified form of biochar produced by nanosizing, exhibits significantly improved adsorption properties due to its enhanced surface area, increased pore volume and higher number of functional groups. These nanoscale modifications result in better accessibility to pollutants, faster adsorption rates and higher adsorption capacities, making nanobiochar a superior adsorbent for wastewater treatment compared to conventional biochar [13,14].

One of the most promising sources for producing high-performance nanobiochar is coconut shells, a widely available, renewable biomass that is typically under utilised. Coconut shells are composed of lignocellulosic material, rich in carbon and possess favourable characteristics for biochar production including a relatively high carbon content and low ash content [15]. By subjecting coconut shells to controlled pyrolysis and subsequent activation, it is possible to develop nanobiochar with a high surface area, extensive porosity and a variety of functional groups that can interact effectively with dye molecules. Furthermore, the transformation of coconut shell into nanobiochar also aligns with the principles of circular economy, as it provides a sustainable solution to both waste management and environmental pollution. The development of coconut shell-derived nanobiochar for dye removal offers a dual benefit: it addresses the global challenge of dye pollution while also providing a means of utilising agricultural waste in a productive manner [16]. This study focuses on the synthesis, characterisation and performance evaluation of coconut shell-derived nanobiochar for the removal of Congo red (CR) and malachite green (MG) from aqueous solutions. These two dyes were selected due to their widespread use and environmental impact, with Congo red being an anionic dye and malachite green a cationic dye, allowing for the investigation of the nano-biochar ability to adsorb both types of pollutants. Nanobiochar was synthesised through controlled pyrolysis of coconut shell biomass, followed by chemical activation to enhance surface area, porosity and nanosizing to improve adsorption performance. The material was characterised using SEM for surface morphology, XRD for structural analysis, DLS for particle size distribution and FTIR to identify the surface functional groups. The study further evaluates adsorption performance by optimizing equilibrium capacity, kinetics and thermodynamic characteristics.

EXPERIMENTAL

Coconut shells used for the preparation of NBC were sourced locally from Chennai city, India. Analytical-grade malachite green (MG) and Congo red (CR) dyes were procured from HiMedia Laboratories (Mumbai, India). Potassium hydroxide (KOH, ≥ 85%), hydrochloric acid (HCl, 37% w/v) and ethanol (99.5% v/v) were obtained from Merck Ltd., India, while Milli-Q deionised water (18.2 MΩ·cm) was used throughout the experiments. All reagents were of analytical grade and used without further purification.

Feedstock preparation: Mature coconut shells were collected from local sources, washed with tap water to remove surface impurities and air-dried for 48 h. The dried shells were manually broken into ~5 mm pieces, milled lightly with a mortar and pestle and sieved to obtain particles of 2-4 mm [17].

Preparation of nanobiochar: Coconut shell particles (50 g) was pyrolysed in a covered ceramic crucible using a laboratory muffle furnace at a ramp rate of 10 ºC min^{-1} to 500 ºC, held for 2 h and allowed to cool inside the furnace to room temperature, yielding raw biochar [18]. The biochar was chemically activated by mixing with KOH at a 1:1 weight ratio in 100 mL of deionised water, stirred for 4 h at room temperature, dried at 80 ºC overnight and reheated at 500 ºC for 1 h. The activated product was washed thoroughly with 0.1 M HCl until neutral pH, rinsed with deionised water and oven-dried at 80 ºC for 12 h to obtain activated biochar [19].

To reduce particle size, the dried activated biochar was subjected to planetary ball milling at 300 rpm for 4 h using zirconia jars and balls to achieve nanoscale dimensions [20]. The milled powder was dispersed in ethanol (10 g L^{-1}) and ultrasonicated in a bath sonicator for 1 h to minimize agglomeration. The suspension was then centrifuged at 3000 rpm for 10 min and the supernatant containing well-dispersed nanobiochar was collected. Ethanol was removed using rotary evaporation at 60 ºC and the concentrate was oven-dried at 80 ºC for 6 h, producing the final nanobiochar powder, which was stored in airtight vials for characterisation and adsorption experiments.

Characterisation: The structural and surface properties of the synthesised nanobiochar were characterised using complementary techniques. X-ray diffraction (XRD) was performed with Cu*K*α radiation (λ = 1.5406 Å) at 40 kV and 15 mA, scanning over a 2θ range of 5-100º with a step size of 0.01º. FTIR was conducted in the range of 4000-400 cm^{-1} using

attenuated total reflectance (ATR) mode with a resolution of 4 cm^{-1} to identify functional groups associated with surface chemistry. Dynamic light scattering (DLS) was employed at 25 ºC to measure hydrodynamic particle size distribution, polydispersity index (PDI) and zeta potential, which provided insights into colloidal stability in aqueous media. Scanning electron microscopy (SEM), coupled with energy-dispersive X-ray (EDX) analysis, was also conducted to investigate the surface morphology and elemental composition of the nanobiochar at high magnification. The SEM provided detailed images of particle shape and size, while the EDX analysis allowed for the identification of specific elemental compositions, further elucidating the surface characteristics. This integrated characterisation approach follows the methodology outlined by Mobarak *et al.* [21].

Batch adsorption: The adsorption experiments aimed at evaluating the efficiency of coconut shell derived nanobiochar for the removal of malachite green (MG) and Congo red (CR) dyes were conducted under controlled batch mode conditions. Stock solutions of MG and CR were prepared at 1000 mg/L concentration using deionised water and serially diluted to desired concentrations ranging from 10 to 200 mg/L in accordance with validated protocols [22].

For kinetic studies, 0.05 g of NBC was added into 100 mL of dye solution at an initial concentration of 50 mg/L in a 250 mL Erlenmeyer flask. The suspensions were agitated in an orbital shaker (150 rpm) at 25 ºC for predetermined time intervals of 5, 15, 30, 60, 120 and 180 min. After shaking, the suspensions were centrifuged at 5000 rpm for 10 min and the supernatant was filtered through a 0.45 µm membrane filter. The residual dye concentration was measured using a UV-vis spectrophotometer at the respective maximum absorption wavelengths (λ_{max} = 497-500 nm for CR and 615-620 nm for MG) as reported by Thakur & Chadar [18].

Adsorption isotherm experiments were conducted by varying the initial concentrations of MG and CR solutions from 10 to 200 mg/L at three temperatures (25, 35 and 45 ºC) to investigate equilibrium adsorption. Each flask contained 0.05 g NBC and 100 mL of dye solution and the suspensions were shaken at 150 rpm until equilibrium was reached.

The influence of solution pH on dye adsorption was examined at pH 3, 5, 7, 9 and 11. The initial pH of the dye solutions was adjusted with 0.1 M HCl or 0.1 M NaOH before adding the adsorbent. Unless otherwise stated, the adsorbent dosage was 0.05 g in 100 mL dye solution (0.5 g L^{-1}) at 25 ºC, with an initial dye concentration of 50 mg L^{-1} [19]. In each experiment, appropriate control samples (without NBC or without dye) were prepared to exclude non-adsorptive losses. All experiments were performed in triplicate and the average values are reported.

Adsorption calculations: The adsorption capacity at time t (q_t) and at equilibrium (q_e) was calculated from dye concentrations as:

$$q_t = \frac{(C_o - C_e) \times V}{M} \quad (1)$$

$$q_e = \frac{(C_o - C_e) \times V}{M} \quad (2)$$

Removal efficiency (%) was computed by:

$$\text{Removal (\%)} = \frac{C_o - C_e}{C_o} \times 100 \quad (3)$$

where C_o and C_e represent initial and equilibrium dye concentrations (mg/L); V is solution volume (L); and M is adsorbent mass (g).

Kinetic models: To describe adsorption rates, kinetic data were fitted to the pseudo-first-order (PFO) [21], pseudo-second-order (PSO) models.

PFO: $$\ln(q_e - q_t) = \ln q_e - K_1 t \quad (4)$$

PSO: $$\frac{t}{q_t} = \frac{1}{K_2 q_e^2} + \frac{t}{q_e} \quad (5)$$

where k_1 (min^{-1}) and k_2 (g mg^{-1} min^{-1}) are kinetic constants. The best-fitting model was identified based on correlation coefficients (R^2) and error analysis (RMSE, χ^2).

Isotherm models: Equilibrium adsorption data were modelled using Langmuir and Freundlich isotherms to describe monolayer adsorption capacity and surface heterogeneity, respectively.

Langmuir:

$$\frac{C_e}{q_e} = \frac{1}{q_{max} K_L} + \frac{C_e}{q_{max}} \quad (6)$$

Freundlich:

$$\log q_e = \log K_f + \frac{1}{n} \log C_e \quad (7)$$

where q_{max} (mg g^{-1}) is the maximum adsorption capacity, K_L (L mg^{-1}) the Langmuir constant and K_F (mg g^{-1}) and 1/n the Freundlich constants describing surface heterogeneity.

Thermodynamic parameters: The distribution coefficient (K_d) was calculated as $K_d = q_e/C_e$. Thermodynamic parameters were derived using:

$$\Delta G^o = -RT \ln K_d \quad (8)$$

$$\ln K_d = \frac{\Delta H^o}{RT} + \frac{\Delta S^o}{R} \quad (9)$$

where R (8.314 J mol^{-1} K^{-1}) is the universal gas constant and T (K) the absolute temperature. Gibbs free energy change (ΔG^o) indicated spontaneity, while enthalpy (ΔH^o) and entropy (ΔS^o) were derived from temperature-dependent studies to infer the nature of the adsorption process [19]. The Model fitting suitability was evaluated through correlation coefficients and error analysis to ensure methodological rigor.

RESULTS AND DISCUSSION

XRD studies: The XRD diffractogram of coconut shell derived nanobiochar (NBC) showed a broad diffraction hump within 20-30º (2θ), characteristic of an amorphous carbon structure with limited long-range order (Fig. 1). The most intense reflection was observed at 24.14º (d = 3.68 Å, 100% intensity), accompanied by a shoulder at 26.11º (d = 3.41 Å, 80%), which corresponded to the (002) plane of turbostratic/disordered graphite. Additional weak reflections at 40.10º and 44.67º were attributed to the (100) and (101) planes of

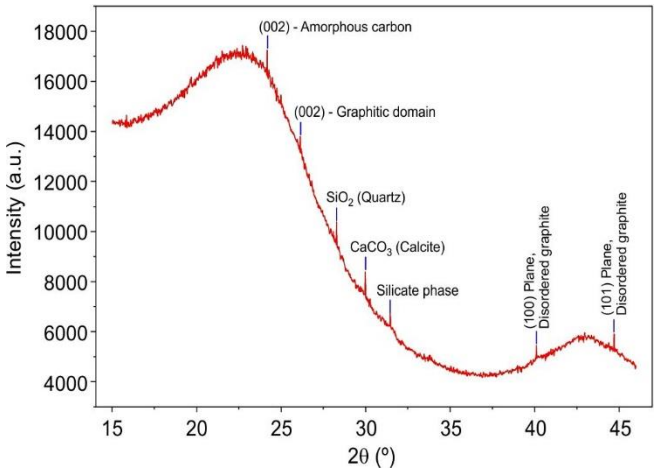

Fig. 1. X-ray diffraction pattern of coconut shell–derived nanobiochar showing characteristic peaks for turbostratic carbon structure and mineral phases

graphite, confirming the presence of nanographitic domains within the amorphous structure. Minor peaks at 28.28º, 29.96º and 31.42º were assigned to silica (SiO_2) and calcite ($CaCO_3$) phases, likely originating from the biomass precursor. These results confirm that NBC is mainly amorphous, with embedded graphitic regions and residual mineral inclusions, consistent with previous studies on coconut shell derived biochars [23,24].

FTIR studies: The FTIR spectrum of nanobiochar displays clear absorption peaks between 1543.1 cm^{-1} and 2952.1 cm^{-1}, with each peak corresponding to particular molecular vibrations that provide valuable information about its chemical structure (Fig. 2). The peak identified at 1543.1 cm^{-1} is associated with C=C stretching vibrations, linked to hemicellulose components present in the biochar [25]. A prominent band at 1684.8 cm^{-1}, is linked to the C=O stretching vibrations carbonyl groups [26]. Moreover, a subtle absorption at 1994.1 cm^{-1} is due to C≡N stretching vibrations [27] indicating the existence of nitrile groups within the nanobiochar. The absorption band at 2340.8 cm^{-1} corresponds to C=O stretching in ketene structures [25]. In the aliphatic region, a peak at 2670 cm^{-1} corresponds to C–H bending vibrations, suggesting alterations in the aliphatic structures throughout the pyrolysis process [25]. The C–H stretching vibrations at 2877.5 cm^{-1} and 2952.1 cm^{-1}, commonly linked to aliphatic groups in cellulose and lignin, exhibit a significant reduction in both biochar and nanobiochar. This reduction indicates the transformation of aliphatic structures into more stable, aromatic forms, as observed by Adawiyah *et al.* [28]. The FTIR findings indicate the structural changes in nanobiochar during pyrolysis, emphasising the transition from aliphatic and hemicellulosic structures to more stable, aromatic and carbonyl-functionalised forms.

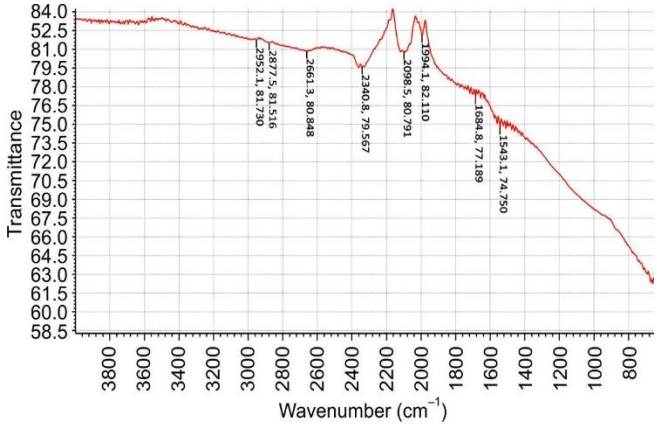

Fig. 2. FT-IR spectrum of nanobiochar displaying functional group assignments and surface chemistry characteristics

DLS analysis: Dynamic light scattering (DLS) confirmed that NBC particles were nanosised with good dispersion stability (Fig. 3). The average hydrodynamic diameter was 27.2 nm (range: 15-45 nm), indicating successful reduction of bulk biochar into the nanoscale regime (Table-1). The polydispersity index (PDI) of 0.23 (0.18-0.30) reflected a moderately narrow particle size distribution, consistent with uniform dispersion. The zeta potential of –30.8 mV (–25 to –38 mV) demonstrated a stable negative surface charge imparted by oxygenated functional groups (–COOH, –OH), which generates the electrostatic repulsion to prevent aggregation. Such colloidal stability maximizes exposed surface area and enhances interactions between nanobiochar and dye molecules, thereby improving adsorption efficiency [20].

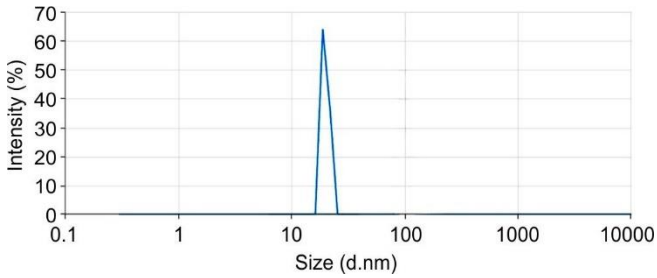

Fig. 3. Dynamic light scattering analysis showing particle size distribution, polydispersity index and zeta potential measurements of nanobiochar suspension

SEM coupled with EDX of coconut shell derived nanobiochar: The SEM and EDX analysis of coconut shell derived nanobiochar provides critical insights into the surface morphology and elemental composition of material. The SEM images at magnifications of 1.98 KX and 8.07 KX reveal a granular, irregularly shaped particle structure, characteristic of high surface area biochars (Fig. 4a-b). The particles exhibit rough, fragmented surfaces with visible cracks, enhancing the poro-

TABLE-1
DLS PARAMETERS OF COCONUT SHELL–DERIVED NANOBIOCHAR

Parameter	Value (typical)	Interpretation
Hydrodynamic diameter (nm)	27.2 (15–45)	Confirmed nanoscale particle size
Polydispersity index (PDI)	0.23 (0.18–0.30)	Moderately narrow size distribution
Zeta potential (ζ, mV)	–30.8 (–25 to –38)	Negative charge ensures colloidal stability

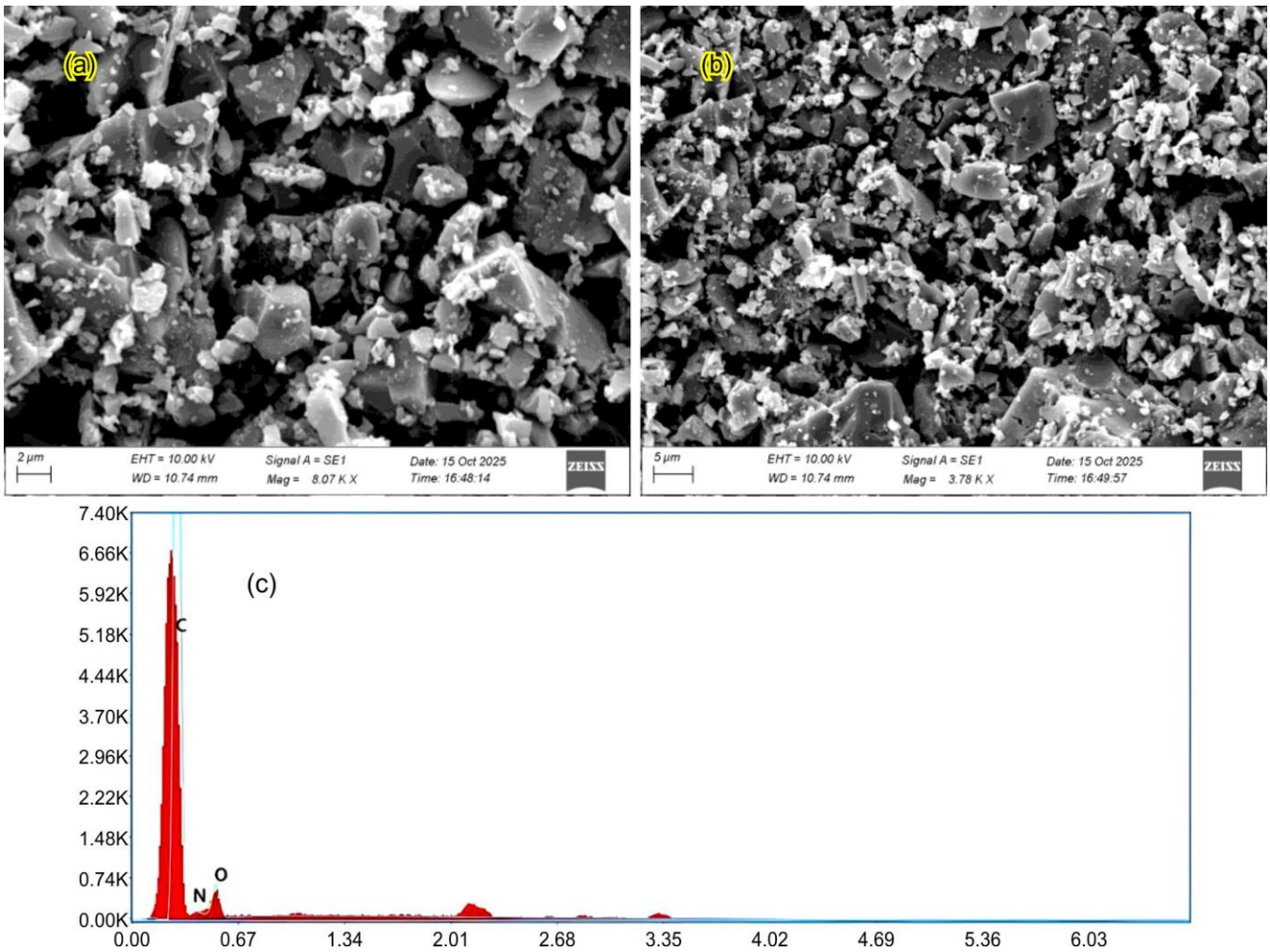

Fig. 4. (a) SEM image of coconut shell-derived nanobiochar at magnification 1.98 KX showing granular and irregular particle morphology, (b) SEM image of coconut shell-derived nanobiochar at magnification 8.07 KX highlighting surface roughness and porosity and (c) EDX spectrum of coconut shell-derived nanobiochar showing elemental composition with peaks for carbon (C), oxygen (O) and nitrogen (N)

sity of the NBC material. Such a morphology is advantageous for adsorption applications, providing abundant active sites for interactions with contaminants. The observed size distribution is heterogeneous, suggesting a varied surface area, which further supports its potential in diverse environmental applications such as water purification and heavy metal removal [29].

The EDX spectrum confirms the elemental composition of the NBC material, with the following approximate atomic percentages: carbon (C) at 87.52%, oxygen (O) at 9.75% and nitrogen (N) at 2.73% as shown in Fig. 4c. The high intensity of the carbon peak is indicative of the carbon-rich nature of the nanobiochar, while the oxygen peak suggests surface oxygenated functional groups, enhancing the reactivity and adsorption capacity of nanobiochar (NBC) materials. The nitrogen peak, though minor, implies the presence of nitrogen containing groups, which may enhance selectivity for specific pollutants. This elemental composition supports the functionality of nanobiochar in adsorptive processes, particularly for polar and nitrogenous contaminants [30]. These structural and compositional characteristics confirm the suitability of the nanobiochar (NBC) for various environmental and industrial applications.

Calibration and λ_{max} determination: The maximum absorption wavelengths were identified at ~440 nm for malachite green (MG) and ~500 nm for Congo red (CR), consistent with earlier literature [19]. The calibration curves demonstrated excellent linearity ($R^2 > 0.99$), confirming adherence to the Beer-Lambert law and validating the use of absorbance for quantitative dye analysis (Fig. 5a-b).

Adsorption kinetics: The time-dependent adsorption of MG and CR onto NBC material was evaluated at C_o = 50 mg L^{-1} with 0.05 g adsorbent in 100 mL solution. Both dyes showed rapid uptake within the first 30 min, followed by slower adsorption until equilibrium was reached. MG attained 88% removal at 120 min, whereas CR achieved 82% removal after 180 min (Table-2).

Kinetic model fitting indicated that the PSO model gave the best correlation ($R^2 \approx 0.99$), suggesting chemisorption as the rate-limiting step, while PFO fits were weaker (Fig. 6). The intraparticle diffusion plots suggested a multi-stage adsorption mechanism, with rapid external diffusion followed by slower pore diffusion.

Adsorption isotherms: Equilibrium adsorption was studied by varying C_o from 10-200 mg/L at 25 ºC. Both dyes

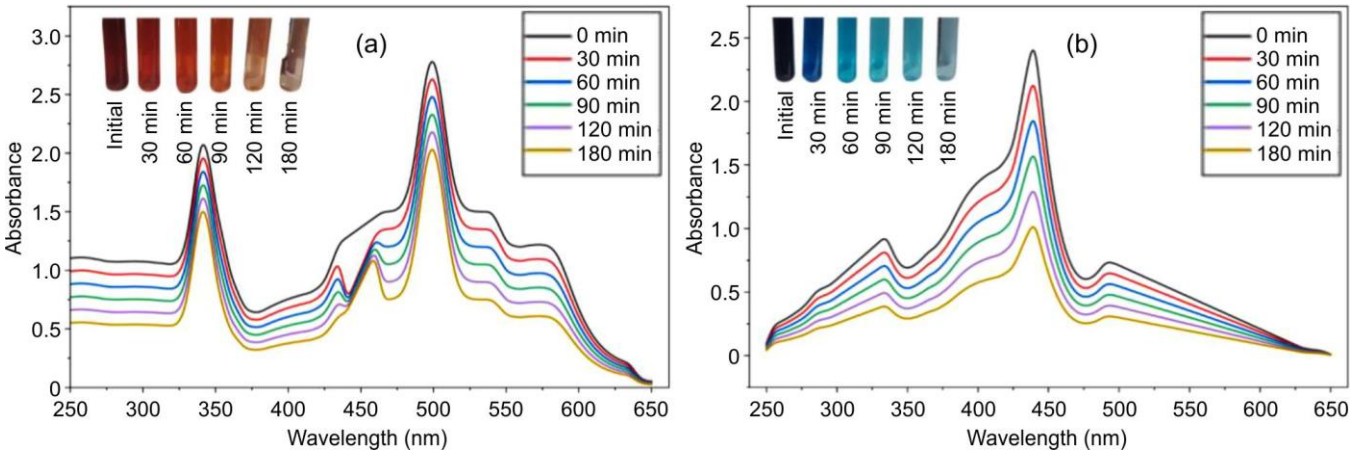

Fig. 5. (a) Time-resolved UV-vis spectra of Congo red during adsorption on nanobiochar, (b) time-resolved UV-vis spectra of malachite green during adsorption on nanobiochar

TABLE-2
ADSORPTION KINETICS DATA OF MALACHITE GREEN (MG) AND CONGO RED (CR) ONTO NANOBIOCHAR (NBC) (C_o = 50 mg/L, V = 100 mL, DOSE = 0.05 g, T = 25 ºC)

Time (min)	C_t (MG, mg/L)	q_t (MG, mg/g)	Removal (%)	C_t (CR, mg/L)	q_t (CR, mg/g)	Removal (%)
5	38	24.0	24.0	42	16.0	16.0
15	28	44.0	44.0	34	32.0	32.0
30	20	60.0	60.0	26	48.0	48.0
60	12	76.0	76.0	18	64.0	64.0
120	8	84.0	84.0	12	76.0	76.0
180	6	88.0	88.0	9	82.0	82.0

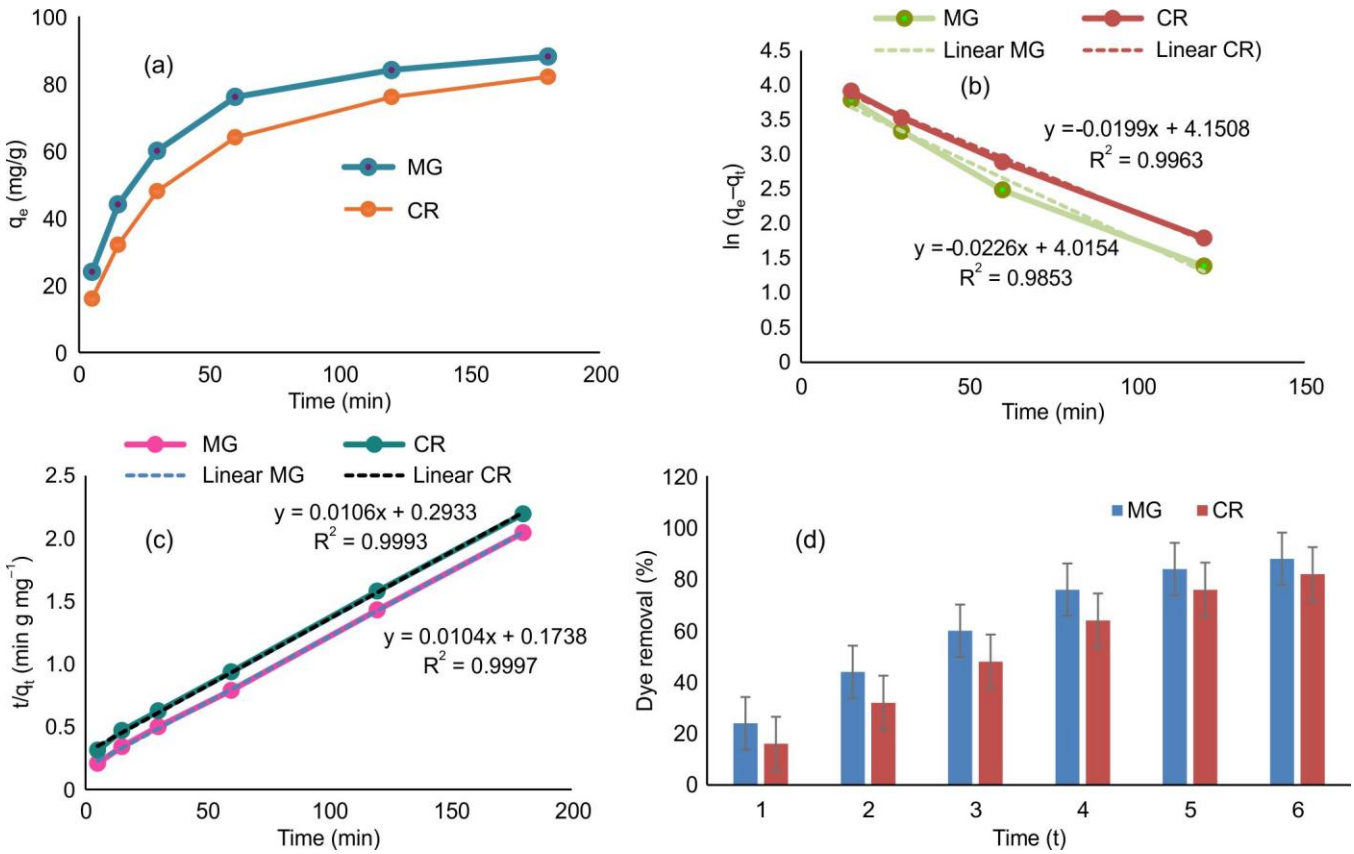

Fig. 6. (a) Time-dependent adsorption profiles of malachite green and Congo red on nanobiochar; (b) pseudo-first-order kinetic model linearisation; (c) pseudo-second-order kinetic model linearisation with correlation coefficients and (d) dye removal percentage of nanobiochar

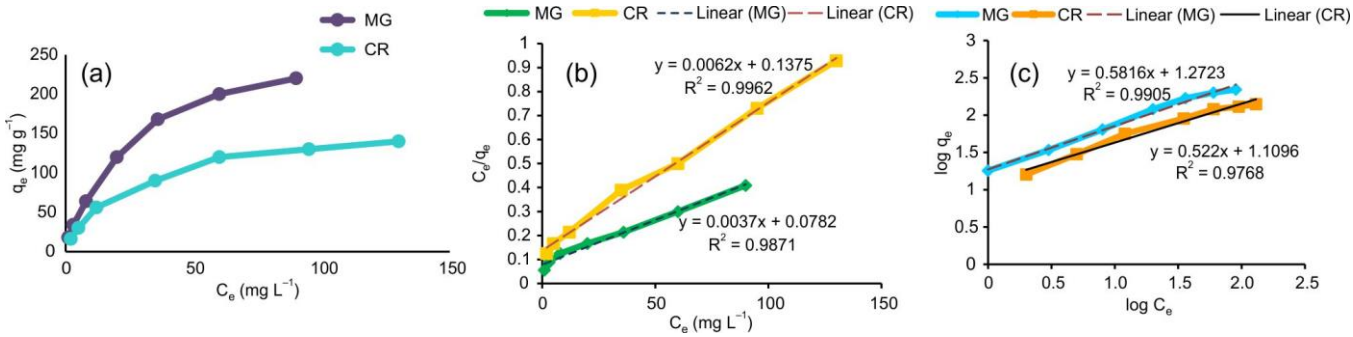

Fig. 7. Isotherm plots at 25 ºC: (a) q_e *vs.* C_e, (b) Langmuir C_e/q_e *vs.* C_e, (c) Freundlich log q_e *vs.* log C_e

exhibited increasing q_e with concentration, approaching saturation at higher loads. MG achieved a maximum of ~220 mg/g, while CR reached ~140 mg/g (Table-3).

TABLE-3
ADSORPTION ISOTHERMS OF MG AND CR ONTO NBC AT 25 ºC (DOSE = 0.05 g, V = 100 mL)

C_o (mg/L)	C_e (MG, mg/L)	q_e (MG, mg/g)	C_e (CR, mg/L)	q_e (CR, mg/g)
10	1	18.0	2	16.0
20	3	34.0	5	30.0
40	8	64.0	12	56.0
80	20	120.0	35	90.0
120	36	168.0	60	120.0
160	60	200.0	95	130.0
200	90	220.0	130	140.0

Langmuir fitting showed MG adsorption followed the monolayer mechanism ($q_{max} \approx 230$ mg/g, $R^2 \approx 0.99$), whereas CR was better described by the Freundlich model ($R^2 \approx 0.96$) (Fig. 7), suggesting the heterogeneous and multilayer binding.

Effect of pH: The adsorption efficiency was highly pH dependent. MG removal increased from 52% at pH 3 to 93% at pH 11, reflecting stronger attraction between the negatively charged surface of NBC material and cationic MG under alkaline conditions. In contrast, CR removal peaked at 81% under acidic conditions (pH 5) and declined with pH rise, consistent with electrostatic repulsion at higher pH (Fig. 8).

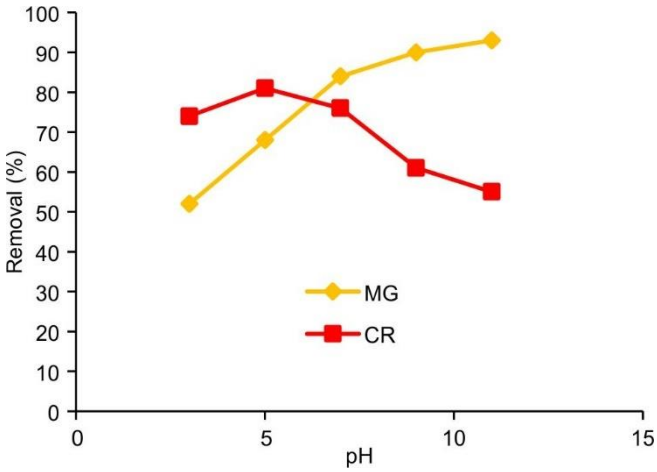

Fig. 8. Effect of solution pH on dye removal efficiency for malachite green and Congo red showing optimal pH ranges for maximum adsorption

Effect of adsorbent dosage: At 0.01 g NBC, MG and CR removal were only 40% and 32%, respectively, while at 0.20 g removal reached ~99% and ~95% (Fig. 9). However, adsorption capacity per gram declined at higher dosages due to overlapping and unsaturated sites, therefore confirmed that absorbent dosage significantly affected the removal of dyes.

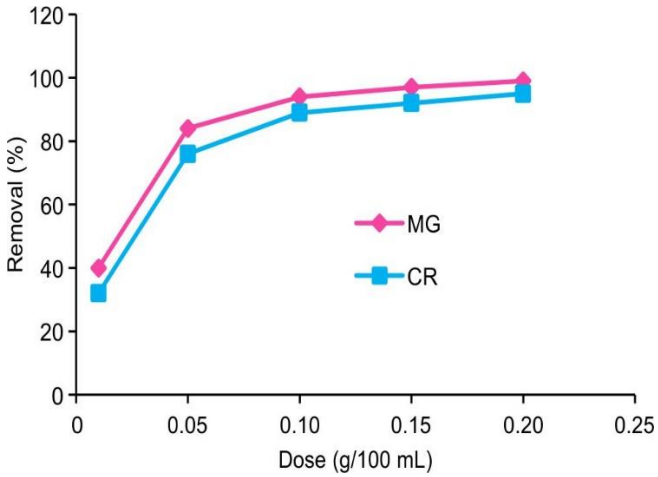

Fig. 9. Influence of nanobiochar dosage on percentage removal and adsorption capacity for both target dyes

Thermodynamic studies: Temperature had a significant effect on the adsorption capacity. The equilibrium adsorption capacity (q_e) for MG increased from 80 to 95 mg g^{-1} as temperature increased from 25 to 45 ºC, while CR adsorption increased from 65 to 78 mg g^{-1} (Table-4). Thermodynamic parameters derived from Van't Hoff analysis (Fig. 10) showed positive enthalpy changes (ΔH^o = 22.5 kJ mol^{-1} for MG and 18.3 kJ mol^{-1} for CR) and positive entropy changes (ΔS^o = 120 J mol^{-1} K^{-1} for MG and +105 J mol^{-1} K^{-1} for CR). The negative Gibb's free energy (ΔG^o) values at the studied temperatures confirm the spontaneous nature of adsorption, while the positive ΔH^o values indicate that the process is endothermic.

TABLE-4
THERMODYNAMIC PARAMETERS FOR MG AND CR ADSORPTION (C_o = 100 mg/L, DOSE = 0.05 g, V = 100 mL)

Temp (ºC)	q_e (MG, mg/g)	q_e (CR, mg/g)	ΔG^o (MG, kJ/mol)	ΔG^o (CR, kJ/mol)
25	80	65	–14.2	–12.5
35	88	72	–15.5	–13.8
45	95	78	–16.8	–14.6

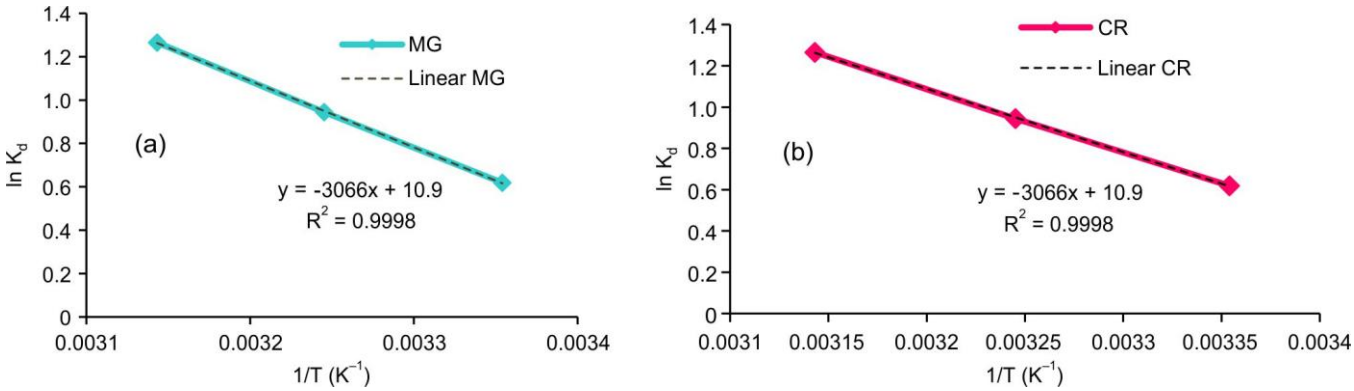

Fig. 10. Van't Hoff plots for thermodynamic parameter determination showing the relationship between ln K_d and 1/T for malachite green and Congo red dyes

Comparison with reported adsorption studies: The adsorption performance of coconut shell derived nanobiochar was evaluated through comparison with previously reported nanobiochar and nano-modified biochar systems in the literature. Table-5 summarizes adsorption capacities, experimental conditions and references for various adsorbent-dye systems.

As shown in Table-5, the adsorption capacity of coconut shell nanobiochar (~220 mg g^{-1} for MG; ~140 mg g^{-1} for CR) is competitive with or superior to several other reported systems. Particularly, the capacities such as 854.75 mg g^{-1} for ball-milled biomass fly ash biochar [34] and ≈354 mg g^{-1} for ball-milled bagasse nanobiochar [38] illustrate the performance gains from nanoscale/ball-milling strategies, while 344.8 mg g^{-1} for nMOSAB toward indigo carmine [31] and a column Q_{max} ≈ 118.06 mg g^{-1} on nZVI-coated corncob biochar [36] show the strong batch and practical fixed-bed results. Nevertheless, the coconut shell nanobiochar demonstrates balanced performance with sustainable feedstock and favourable regeneration properties, supporting its practical viability.

Conclusion

In conclusion, the coconut shell-derived nanobiochar (NBC), engineered through mild activation and nanoscale size reduction, demonstrates fast and efficient removal of both cationic (MG) and anionic (CR) dyes. The surface chemistry of NBC with oxygenated/aromatic groups, dispersibility and nano-scale morphology enable high adsorption rates and capacities, with MG fitting Langmuir monolayer behaviour (q_{max} ~230 mg g^{-1}) and CR following Freundlich (heterogeneous sites). PSO kinetics ($R^2 \approx 0.99$) and positive enthalpies confirm chemi-sorption-dominated, endothermic uptake; negative ΔG^o across 25-45 ºC indicates spontaneity. The higher MG removal

TABLE-5
COMPARATIVE ADSORPTION CAPACITIES AND EXPERIMENTAL CONDITIONS OF NANOBIOCHAR AND NANO-MODIFIED BIOCHAR ADSORBENTS FOR VARIOUS DYE REMOVAL

Dye removed	Adsorbent (nanobiochar/ nano-modified biochar)	Adsorption capacity (q_{max} or q_e, mg g^{-1})	Conditions	Ref.
Congo red (CR)	Areca catechu nano-biochar	154.53	0.02 g/20 mL, C_o = 50 mg L^{-1}, pH ≈ 5, 303-333 K, 180 min	[28]
Indigo carmine	Nano-activated biochar derived from Moringa oleifera seeds (nMOSAB)	344.8	pH = 4, contact time = 90 min, adsorbent dose = 100 mg	[31]
Rhodamine B (RhB)	Water-washed coffee-shell biochar (nanostructured surface)	147.6–193.5	0.05 g/100 mL, C_o = 50-300 mg L^{-1}, pH 7 (opt. neutral), 25-45 ºC, ≈180 min to equilibrium; batch mode.	[32]
Methylene blue (MB)	Ball-milled rice-straw nano-biochar (BRB)	50.27	Optimised at pH 8, 40 ºC, 90 min	[33]
Methylene blue (MB)	Ball-milled biomass fly ash/biochar composite (nano-scaled)	854.75	Batch isotherms at 318 K, pH 4-10; C_o (typ.) 20-300 mg L^{-1}	[34]
malachite green (MG)	Rice husk nano-biochar (ultrasonication/centrifugation)	216–351	0.05 g/100 mL, C_o = 50 mg L^{-1} (typ.), pH 1.8-9.8 (capacity with pH to ~6-7), 25 ºC; batch shaking per methods.	[35]
Methylene blue (MB)	nZVI-coated corncob biochar (nano-zero-valent iron on BC; fixed-bed column)	118.06	Mode: fixed-bed; bed height: 2 cm; adsorbent mass: 1.0 g; flow: 10 mL min^{-1}; C_o: 100 mg L^{-1}; pH: 7 (MB single-dye); T: room temp.	[36]
Rhodamine B (RhB)	Nano iron-oxide–modified biochar (CBC-Fe(II)) from microalgae	289.6	Batch; adsorbent mass = 30 mg in 25 mL (≈1.2 g L^{-1}), 25 ºC, 120 min; Langmuir fit; magnetic separation	[37]
Methylene blue (MB)	Ball-milled bagasse biochar (nano-scaled)	354	0.10 g/100 mL, C_o = 10–500 mg L^{-1}, 25 ºC, pH ≈ 6.5-7.0, 24 h (equilibrium)	[38]

at higher pH, maximal CR removal near mildly acidic pH and increasing removal with dose are consistent with electrostatic/π-π interactions occurring on the graphitised domains of NBC material. From an application perspective, the biomass origin, simple synthesis, and strong adsorption performance of NBC support its potential use in dye-contaminated wastewater treatment.

CONFLICT OF INTEREST

The authors declare that there is no conflict of interests regarding the publication of this article.

DECLARATION OF AI-ASSISTED TECHNOLOGIES

During the preparation of this manuscript, the authors used an AI-assisted tool(s) to improve the language. The authors reviewed and edited the content and take full responsibility for the published work.

REFERENCES

1. J. Sharma, S. Sharma and V. Soni, *Reg. Stud. Mar. Sci.*, **45**, 101802 (2021); https://doi.org/10.1016/j.rsma.2021.101802
2. Kusumlata, B. Ambade, A. Kumar and S. Gautam, *Limnol. Rev.*, **24**, 126 (2024); https://doi.org/10.3390/limnolrev24020007
3. S. Mihai, A. Bondarev and M. Necula, *Processes*, **13**, 589 (2025); https://doi.org/10.3390/pr13020589
4. S. Rajendran, A. Kalairaj and T. Senthilvelan, *Biomass Convers. Biorefin.*, **15**, 13079 (2025); https://doi.org/10.1007/s13399-024-06104-0
5. A. Kumar, A. Kapoor, A.K. Rathoure, G.L. Devnani and D.B. Pal, *Asia-Pacific J. Chem. Eng.*, **20**, e70122 (2025); https://doi.org/10.1002/apj.70122
6. G. Bal and A. Thakur, *Mater. Today Proc.*, **50**, 1575 (2022); https://doi.org/10.1016/j.matpr.2021.09.119
7. M. Kumar, A. Mishra, S.K. Patel, S. Singh, V. Mishra, D. Singh, V. Singh, B.S. Giri, R.R. Singhania, J. Kushwaha, and D. Singh, *Bioengineering*, **12**, 1043 (2025); https://doi.org/10.3390/bioengineering12101043
8. S. Satyam and S. Patra, *Heliyon*, **10**, e29573 (2024); https://doi.org/10.1016/j.heliyon.2024.e29573
9. F. Bahmanzadegan and A. Ghaemi, *J. Hazard. Mater. Adv.*, **17**, 100617 (2025); https://doi.org/10.1016/j.hazadv.2025.100617
10. A. Tomczyk, Z. Sokołowska and P. Boguta, *Rev. Environ. Sci. Biotechnol.*, **19**, 191 (2020); https://doi.org/10.1007/s11157-020-09523-3
11. G. Infurna, G. Caruso and N. Tz. Dintcheva, *Polymers*, **15**, 343 (2023); https://doi.org/10.3390/polym15020343
12. W.A. Shaikh, A. Kumar, S. Chakraborty, M. Naushad, R.U. Islam, T. Bhattacharya and S. Datta, *Chemosphere*, **308**, 136413 (2022); https://doi.org/10.1016/j.chemosphere.2022.136413
13. T.G. Ambaye, M. Vaccari, E.D. van Hullebusch, A. Amrane and S. Rtimi, *Int. J. Environ. Sci. Technol.*, **18**, 3273 (2021); https://doi.org/10.1007/s13762-020-03060-w
14. V. Jadhav, B. Ahire, A. Pawar, A. Roy, A. Kumar, K. Sharma, S. Raj and R. Verma, *Environ. Nanotechnol. Monit. Manag.*, **23**, 101061 (2025); https://doi.org/10.1016/j.enmm.2025.101061
15. A. Ajien, J. Idris, N. M. Sofwan, R. Husen and H. Seli, *Waste Manag. Res.*, **41**, 37 (2022); https://doi.org/10.1177/0734242X221127167
16. M. Varkolu, S. Gundekari, N. Omvesh, V.C.S. Palla, P. Kumar, S. Bhattacharjee and T. Vinodkumar, *Catalysts*, **15**, 243 (2025); https://doi.org/10.3390/catal15030243
17. R.S. Piriya, R.M. Jayabalakrishnan, M. Maheswari, K. Boomiraj and S. Oumabady, *Water Sci. Technol.*, **83**, 1167 (2021); https://doi.org/10.2166/wst.2021.050
18. D.S. Thakur and S.N. Chadar, *Res. Dev. Mater. Sci.*, **22**, 2707 (2025); https://doi.org/10.31031/RDMS.2025.22.001034
19. W. Fan and X. Zhang, *Environ. Res.*, **269**, 120933 (2025); https://doi.org/10.1016/j.envres.2025.120933
20. J.I. Mnyango, M. Phiri and J. Baloyi, *Sustain. Chem. Pharm.*, **35**, 101074 (2025); https://doi.org/10.1016/j.scp.2025.101074
21. M.B. Mobarak, N.S. Pinky, S. Mustafi, F. Chowdhury, A. Nahar, U.S. Akhtar, M.S. Quddus, S. Yasmin and M.A. Alam, *RSC Adv.*, **14**, 24939 (2024); https://doi.org/10.1039/D4RA05562D
22. R. Mustapha, M. Harun, A. Manas, A. Ali and S. Hamzah, *Biointerface Res. Appl. Chem.*, **11**, 10006 (2020); https://doi.org/10.33263/BRIAC113.1000610015
23. T. Cheng, K. Zhang, J. Guo, Q. Yang, Y. Li, M. Xian and R. Zhang, *Biotechnol. Biofuels Bioprod.*, **15**, 39 (2022); https://doi.org/10.1186/s13068-022-02136-8
24. N.H.L. Nicholas, I. Mabbett, H. Apsey and I. Robertson, *Gates Open Res.*, **6**, 96 (2022); https://doi.org/10.12688/gatesopenres.13727.2
25. M.S. Reza, S. Afroze, M.S. Bakar, R. Saidur, N. Aslfattahi, J. Taweekun and A.K. Azad, *Biochar*, **2**, 239 (2020); https://doi.org/10.1007/s42773-020-00048-0
26. A.M. Al-Omran, M.M. Awad, A.G. Alghamdi and A. Alkhasha, *Appl. Sci.*, **13**, 7781 (2023); https://doi.org/10.3390/app13137781
27. S.S. Royji Albeladi, M.A. Malik and S.A. Al-thabaiti, *J. Mater. Res. Technol.*, **9**, 10031 (2020); https://doi.org/10.1016/j.jmrt.2020.06.074
28. R. Adawiyah, N. Yuliasari, Y. Hanifah and N.R. Palapa, *Bull. Chem. React. Eng. Catal.*, **20**, 112 (2025); https://doi.org/10.9767/bcrec.20322
29. X. Zhang, W. Cheng, J. Wang, Y. Lei, X. Yang, Q. Duan, W. Duan, and Y. Zhang, *Green Process. Synth.*, **13**, 20240154 (2024); https://doi.org/10.1515/gps-2024-0154
30. Z. Li, W. Tong, C. Li, Z. Dong, S. Han, K. Li, J. Wang, J. Qu and Y. Zhang, *Sep. Purif. Technol.*, **354** 129017 (2025); https://doi.org/10.1016/j.seppur.2024.129017
31. M. ElKammah, E. Elkhatib and M. Moubarak, *Appl. Water Sci.*, **15**, 194 (2025); https://doi.org/10.1007/s13201-025-02556-5
32. X. Kan, Y. Suo, B. Shi, Y. Zheng, Z. Liu, W. Ma, X. Li and J. Zhang, *Molecules*, **30**, 2769 (2025); https://doi.org/10.3390/molecules30132769
33. J. Wang, Y. Tan, H. Yang, L. Zhan, G. Sun and L. Luo, *Sci. Rep.*, **13**, 21174 (2023); https://doi.org/10.1038/s41598-023-48373-1
34. H. Li, J. Kong, H. Zhang, J. Gao, Y. Fang, J. Shi, T. Ge, T. Fang, Y. Shi, R. Zhang, N. Zhang, X. Dong, Y. Zhang and H. Li, *J. Water Process Eng.*, **53**, 103713 (2023); https://doi.org/10.1016/j.jwpe.2023.103713
35. S. Aziz, B. Uzair, M.I. Ali, S. Anbreen, F. Umber, M. Khalid, A.A. Aljabali, Y. Mishra, V. Mishra, Á. Serrano-Aroca, G.A. Naikoo, M. El-Tanani, S. Haque, A.G. Almutary and M.M. Tambuwala, *Environ. Res.*, **238**, 116909 (2023); https://doi.org/10.1016/j.envres.2023.116909
36. W. Ding, A. Habineza, X. Zeng, Z. Yan, J. Yan and G. Yang, *Desalination Water Treat.*, **260**, 169 (2022); https://doi.org/10.5004/dwt.2022.28445
37. Z. Peng, Z. Fan, X. Chen, X. Zhou, Z.F. Gao, S. Deng, S. Wan, X. Lv, Y. Shi and W. Han, *Nanomaterials*, **12**, 2271 (2022); https://doi.org/10.3390/nano12132271
38. H. Lyu, B. Gao, F. He, A.R. Zimmerman, C. Ding, J. Tang and J.C. Crittenden, *Chem. Eng. J.*, **335**, 110 (2018); https://doi.org/10.1016/j.cej.2017.10.130